Available online at www.sciencedirect.com

ScienceDirect

Geochimica et Cosmochimica Acta 275 (2020) 1–18

Geochimica et Cosmochimica Acta

www.elsevier.com/locate/gca

Barium isotope systematics of subduction zones

Sune G. Nielsen [a,b,*], Yunchao Shu [a,c], Maureen Auro [a], Gene Yogodzinski [d], Ryuichi Shinjo [e], Terry Plank [f], Suzanne M. Kay [g], Tristan J. Horner [a,h]

[a] NIRVANA Labs, Woods Hole Oceanographic Institution, 02543 Woods Hole, MA, USA
[b] Department of Geology and Geophysics, Woods Hole Oceanographic Institution, 02543 Woods Hole, MA, USA
[c] School of Earth and Space Sciences, University of Science and Technology of China, Hefei, Anhui 230026, China
[d] Department of Earth and Ocean Sciences, University of South Carolina, Columbia, SC, USA
[e] Department of Physics and Earth Sciences, University of the Ryukyus, Senbaru 1, Nishihara, Okinawa 903-0213, Japan
[f] Lamont Doherty Earth Observatory, Columbia University, NY, USA
[g] Department of Earth and Atmospheric Sciences, Cornell University, Ithaca, NY, USA
[h] Department of Marine Chemistry and Geochemistry, Woods Hole Oceanographic Institution, 02543 Woods Hole, MA, USA

Received 9 September 2019; accepted in revised form 5 February 2020; Available online 14 February 2020

Abstract

Subduction zones are the focal points of mass transfer between the surface and deep Earth. Despite their significance, there remains substantial debate regarding the specific mechanisms of material transport from the slab to the overlying magmatic arc. Broadly, models accounting for slab material transport focus on the relative sequence of events promoting arc volcanism and, in particular, whether mobilization of the down-going slab leads or lags mixing with the mantle wedge. To address these uncertainties, we outline the utility of barium (Ba) isotope mass balance in subduction zones as a means to test different slab material transport models. Barium is a highly fluid-mobile element that is significantly enriched in arc magmas and is thus thought to be a sensitive tracer of slab material transport in arcs.

We also present qualitative Ba isotopic mass balances for two well-characterized subduction zones—the Aleutian and Ryukyu magmatic arcs—by analyzing the Ba isotope systematics of their respective subduction inputs and outputs. Despite the narrow (and similar) Ba-isotope range of slab inputs to both systems, we find that erupted magmas exhibit systematic variations indicative of a small negative isotope fractionation during Ba mobilization (≈20–40 ppm AMU^{-1}). We suggest that AOC (altered oceanic crust) is not the principal source of these negative isotope values using other geochemical parameters (e.g., Rb/Ba, Pb isotopes), and infer that the Ba isotope composition of AOC—though contributing a minor amount of Ba in these systems—is isotopically heavier than the overlying sediment package and the depleted mantle. Altogether, these findings are significant as they indicate that the magnitude of isotope fractionation associated with Ba mobilization is small relative to the likely isotopic contrast between subduction inputs in other subduction zones, such as beneath areas of strong ocean upwelling (e.g., South Sandwich, Kamchatka). Thus, we propose that the Ba isotope composition of erupted arc magmas holds great promise for constraining the importance of different slab components, which could help address uncertainties regarding the mechanism of slab material transport in subduction zones.

Keywords: Magma; Mantle; Arc; Slab material transport; Fluids; Sediments; Altered oceanic crust

1. INTRODUCTION

The fundamental physical processes that control the transfer of material from subducted slabs to the Earth's

* Corresponding author at: NIRVANA Labs, Woods Hole Oceanographic Institution, 02543 Woods Hole, MA, USA.
E-mail address: snielsen@whoi.edu (S.G. Nielsen).

https://doi.org/10.1016/j.gca.2020.02.006
0016-7037/

surface remain uncertain. One of the best means of studying these processes is to compare the chemical and isotopic compositions and fluxes of what goes into a subduction zone (sediments and hydrothermally altered ocean crust (AOC)) with those of arc magmas, which are the most prominent output fluxes of these large systems.

Geochemical evidence suggests that both subducted sediment and AOC play significant roles in the chemical signatures of arc magmas (e.g. Kay et al., 1978; Tera et al., 1986; Plank and Langmuir, 1993; Ishikawa and Nakamura, 1994; Elliott et al., 1997). However, the mechanisms by which these components are transported from the slab to the surface are still debated. Some models suggest that the general structure of the subducted slab remains sufficiently intact through a large portion of the subduction process that when the slab becomes hot enough to melt sediments and dehydrate AOC, these discreet components are released to the mantle wedge and induce melting (Tatsumi, 1989; Elliott et al., 1997). Experiments involving sediments at pressures and temperatures relevant for the top of the subducted slab (i.e. 2–4 GPa and 600–1000 °C) have shown that fluids released from sediments during dehydration do not contain high trace element abundances (Spandler et al., 2007) whereas partial melts extracted from similar sediments contain very high trace element abundances (Hermann and Rubatto, 2009; Johnson and Plank, 1999; Skora and Blundy, 2010). In contrast, fluids originating from dehydrated AOC also contain high trace element abundances and both these and sediment melts exhibit many of the trace element fractionations observed in arc magmas (Carter et al., 2015; Hermann and Rubatto, 2009; Johnson and Plank, 1999; Kessel et al., 2005; Skora and Blundy, 2010). Further, it has been suggested that the breakdown of serpentinite within the lithospheric mantle (likely formed via bending faults under the forearc (Worzewski et al., 2011)) could release water that would extract fluid mobile elements as it percolated through the oceanic crust and carry these elements to the magma forming region (Spandler and Pirard, 2013). However, the amount of serpentine present in the lithospheric mantle is still uncertain as its formation is associated with a large volume increase (Klein et al., 2015) that should arrest the downward fluid flow required to produce it (Korenaga, 2017).

Other models contend that all subducted components are physically mixed at the top of the slab, forming a 'mélange' layer (Fig. 1; (Marschall and Schumacher, 2012; Nielsen and Marschall, 2017)). Melts and fluids are can then be extracted from this mélange layer with some recent experimental studies showing that this processes can produce at least some of the trace element fractionations observed in subduction zones (Codillo et al., 2018; Cruz-Uribe et al., 2018).

The two end-member models of slab material transport are physically distinct (Fig. 1), and have different consequences for the thermal structure and distribution of volcanoes in subduction zones as well as chemical budgets of crustal recycling into the deep Earth. Unfortunately, there are few extant chemical tests that can distinguish between these two models. For example, the chemical compositions of arc magmas derived from either model will display similar fractionated trace-element ratios. Furthermore, both models make similar predictions concerning the presence and detection of small amounts of subducted sediment and/or AOC when using radiogenic isotope tracers, such as $^{87}Sr/^{86}Sr$ and $^{143}Nd/^{144}Nd$.

In both models, fluids are the mediators of slab material transport (Fig. 1), which—together with partial melting of slab material—can explain the trace element fractionation patterns in arc magmas. However, in the first class of end-member models, fluids are sourced primarily via metamorphic dehydration of minerals in AOC, whereas fluids in the second class of end-member models are sourced from the mélange layer that is composed of a mixture of all slab components (Fig. 1). Therefore, any geochemical tracer that is transported via fluids in subduction zones and exhibits systematically different compositions for AOC and sediments has the potential to distinguish between the two end-member models.

Barium (Ba) is a potentially powerful tracer in this regard, as it is highly fluid-mobile (Kessel et al., 2005; Carter et al., 2015) and significant Ba enrichments are observed in many arc magmas worldwide (e.g. Elliott, 2003; Elliott et al., 1997; Kay, 1980). However, interpretation of the origin of high Ba abundances in arc magmas are not possible using only concentrations since fluids in both end-member models would be expected to exhibit Ba enrichments. In contrast, if even a small Ba isotopic difference exists between sediments and AOC, the two models would predict distinct Ba isotopic patterns in the erupted arc magmas depending on whether the Ba budget in the subducted slab was originally dominated by sediments or AOC. As such, the fluids predicted to originate from AOC could have a different Ba isotope composition than the fluids sourced from a mélange as the latter should represent mixtures between sedimentary and AOC-bound Ba.

Here we explore the utility of Ba isotopes in determining fluid sources in subduction zones by reporting the first comprehensive Ba isotope study of arc magmas—focusing on two arcs, Aleutian and Ryukyu—and by reviewing available Ba isotope data from global sediments and AOC. Our new isotopic data illustrate that there is insufficient Ba isotope variation to confidently use Ba isotopes as a tracer of fluid sources in either the Aleutian or Ryukyu arcs. However, this finding does not preclude the use of Ba isotopes as tracers of subduction fluids in other arc settings that possess larger Ba isotope differences between sediments and AOC. Such settings are most likely to be found in the Southern Ocean and northwest Pacific.

2. SCIENTIFIC BACKGROUND

2.1. Barium behavior in arcs

It has long been known that Ba is highly enriched in arc magmas compared with concentrations observed in mid ocean ridge basalts (MORBs) (e.g. Kay, 1980; Plank and Langmuir, 1993). This Ba enrichment must come from a component sourced from the subducted slab—either ser-

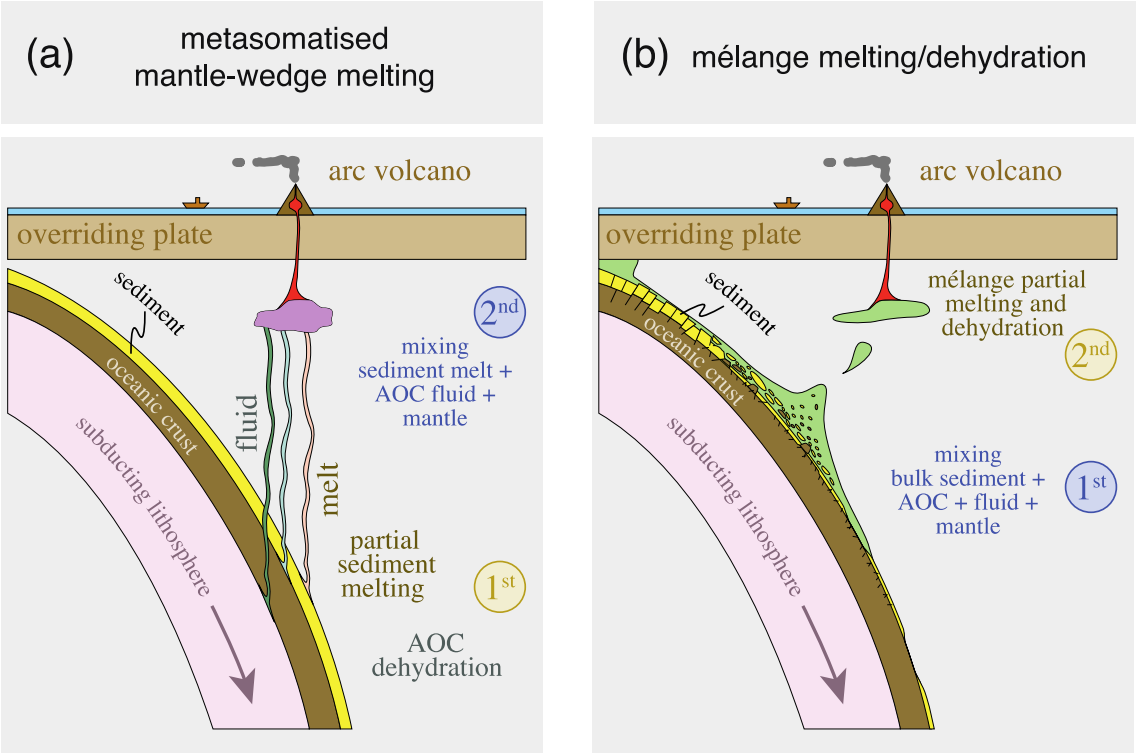

Fig. 1. Cartoons (not to scale) of the two different end-member models of slab material transport in subduction zones (modified from Nielsen and Marschall, 2017). (a) In the standard model, sediment melts and fluids from AOC and/or deeply seated serpentinites, which all display fractionated trace-element signatures, are sourced directly beneath the arc volcano where they percolate rapidly to the region of melting. Here they mix with ambient mantle melts to form arc magmas. (b) In the mélange model, sediments, AOC and hydrated mantle physically mix to form hybrid mélange rocks. The mélange material subsequently rises in diapirs into the mantle wedge and melts to form arc magmas with fractionated trace-element signatures. A critical difference between the two models is that the mixing and slab material transport occurs in reverse order leading to different stable isotopic ratios for high concentration elements with disparate isotope compositions in sediments and AOC.

pentinites, the oceanic crust, or sediments. In addition to the overall high Ba concentrations, the source of the Ba enrichment has been traced by normalizing to elements of similar compatibility such as La or Th (e.g. Elliott, 2003; Elliott et al., 1997; Pearce and Peate, 1995; Woodhead et al., 1998). Ratios of Ba/Th and Ba/La are often significantly higher than what would be observed in average subducted sediment or AOC, which requires addition of Ba in the form of, for example, a fluid with very high Ba/Th or Ba/La ratios (e.g. Pearce and Peate, 1995). Indeed, experiments in which fluids were equilibrated with basaltic ocean crust showed that Ba is substantially more soluble than Th and La in fluids over ranges in temperature (600–1000 °C) and pressure (4–6 GPa) that are relevant for subduction zones (Kessel et al., 2005; Carter et al., 2015). Given these constraints, high Ba/La and Ba/Th ratios in arc magmas are often inferred to reflect addition of a fluid from AOC (Pearce and Peate, 1995; Woodhead et al., 1998; Elliott, 2003).

However, sedimentary Ba concentrations can vary to a very large extent because the mineral barite ($BaSO_4$) controls most of the Ba budget of many marine sediments (Plank and Langmuir, 1998); even minor quantities of barite in a sediment will have a large effect on the bulk Ba concentration. Therefore, some individual sediment horizons rich in barite display very high Ba/La and Ba/Th ratios that exceed the highest ratios observed in arc magmas (e.g. Plank and Langmuir, 1998). Marine barites form as micron-sized crystals that precipitate during heterotrophic oxidation of particulate organic matter in the water column (e.g. Dehairs et al., 1980). These barites are then exported to the seafloor along with other sinking debris, resulting in a strong linear correlation between export productivity and barite mass accumulation rates in marine sediments (e.g. Eagle et al., 2003; Paytan and Griffith, 2007). In addition, barite also precipitates from high temperature hydrothermal fluids and hydrothermal sediments can contain up to two weight % Ba (Plank and Langmuir, 1998). Hence, Ba concentrations in marine sediments depend strongly on the depositional environment and may vary by several orders of magnitude (Plank and Langmuir, 1998). As such, there is still significant uncertainty regarding whether the ultimate source of Ba enrichments in arc magmas originate from $BaSO_4$ in sediments or AOC (Plank and Langmuir, 1993; Elliott et al., 1997). Regardless, the preferential mobilization of Ba relative to Th and

La likely requires a fluid phase or fluid-rich melt to further enrich Ba in resultant arc magmas (Elliott et al., 1997; Kessel et al., 2005; Hermann and Rubatto, 2009; Skora and Blundy, 2010).

2.2. Isotope geochemistry of barium

Studies of high precision stable Ba isotopes were only recently developed, with a landmark paper by Von Allmen et al. (2010) identifying a significant negative isotope fractionation during $BaSO_4$ precipitation at 20–80 °C. Barium isotope compositions have been reported using the conventional delta notation, albeit referenced to different standards and using different sets of isotopes, most commonly $^{138}Ba/^{134}Ba$ or $^{137}Ba/^{134}Ba$. In principle, all these notations reflect the same underlying isotope variation and can be re-calculated to the same notation. For consistency with the majority of the most recent Ba isotope literature, we report variations using the $^{138}Ba/^{134}Ba$ notation relative to the NIST SRM 3104a standard:

$$\delta^{138/134}Ba_{NIST\ 3104A}\,(in\ ‰) = 1000 \times ((^{138}Ba/^{134}Ba_{sample}/^{138}Ba/^{134}Ba_{NIST\ 3104A}) - 1)$$

One of the primary findings of recent Ba isotope studies in low-T environments is that precipitation of barite appears to be the primary mediator of Ba isotope fractionation in the open ocean (e.g. Horner et al., 2015). Specifically, precipitation of barite is associated with a fractionation factor of $\alpha \sim 0.9995 \pm 0.0001$ (e.g. barites are enriched in the light isotopes relative to seawater by ≈ -0.5‰; (Horner et al., 2015, 2017; Bridgestock et al., 2018)). The direction of isotope fractionation is consistent with theoretical calculations (Hofmann et al., 2012) and experiments (von Allmen et al., 2010). The effects of this isotope fractionation causes a distinct structure of Ba isotopes in the ocean whereby the surface ocean in oligotrophic regions (such as the gyres of the South Atlantic or North Pacific) are depleted in Ba (~40 nM/kg; (Chan et al., 1977)) and characterized by heavy Ba isotope compositions of $\delta^{138/134}Ba_{NIST\ 3104A} \approx +0.6$‰ (Horner et al., 2015; Bridgestock et al., 2018), whereas deep waters that are rich in nutrients have higher Ba concentrations (≥100 nM/kg; (Chan et al., 1977)) and $\delta^{138/134}Ba_{NIST\ 3104A} \approx +0.2$ to $+0.3$‰ (Horner et al., 2015; Bridgestock et al., 2018). In regions of the ocean where nutrient concentrations in surface waters are high due to strong upwelling of deep water (such as the Southern Ocean; (Talley, 2013)), lighter Ba isotope values are also observed in the surface ocean. The variation in Ba isotope composition of the near-surface ocean is important because almost all pelagic barite precipitation takes place in the uppermost few hundred meters of the water column (e.g. Jacquet et al., 2008). Given the relatively constant fractionation factor between barite and seawater, marine barites will be characterized by different $\delta^{138/134}Ba_{NIST\ 3104A}$ depending on their geographical location. For example, barites precipitated in the Southern Ocean, where surface waters are rich in nutrients and display light Ba isotope compositions, have been found to exhibit $\delta^{138/134}Ba_{NIST\ 3104A} \sim -0.2$‰ (Crockford et al., 2019), whereas barites from nutrient poor regions, such as the South Atlantic display barite $\delta^{138/134}Ba_{NIST\ 3104A} \sim +0.1$ (Bridgestock et al., 2018)). In turn, these Ba isotope variations in barites are a strong factor controlling the $\delta^{138/134}Ba_{NIST\ 3104A}$ of the subducted sediment package, as barites are often the main Ba-bearing component of pelagic sediments (Plank and Langmuir, 1998).

The Ba isotope composition of AOC is also likely influenced by the Ba isotope systematics of seawater through hydrothermal circulation of seawater at low temperatures. During low-T hydrothermal alteration, Ba is not significantly deposited into secondary minerals or extracted from the oceanic crust (Staudigel and Hart, 1983; Kelley et al., 2003). Similarly to Ba, Sr (strontium) also shows only minor deviation in concentrations from unaltered to altered oceanic crust (Staudigel and Hart, 1983; Kelley et al., 2003), but studies have shown substantial Sr-isotopic exchange and dissolution-precipitation reactions between seawater and ocean crust, such that AOC partially inherits the Sr isotope composition of seawater (e.g. Staudigel and Hart, 1983). These reactions are likely at least partially controlled by precipitation of carbonates and sulfates, both of which can accommodate Ba due to the geochemical similarity of Ca, Sr, and Ba in terms of charge and ionic radius. Therefore, it is expected that similar Ba isotopic exchange also takes place between seawater and the oceanic crust, in which case AOC might be expected to partially inherit the Ba isotope composition of the seawater circulating through it. Given that the range of seawater Ba isotope composition is $\delta^{138/134}Ba_{NIST\ 3104A} \approx +0.3$ to $+0.6$‰ (Horner et al., 2015), it is expected that these compositions form one boundary composition for AOC. This inference appears to be qualitatively confirmed by recent reports of AOC samples from ODP Hole 1256D, ODP Hole 504B and DSDP Hole 442B that displayed values as heavy as $\delta^{138/134}Ba_{NIST\ 3104A} = +0.4$‰ (Nielsen et al., 2018). The other end of the AOC spectrum is likely represented by the Ba isotope composition of unaltered MORBs, which display values between $\delta^{138/134}Ba_{NIST\ 3104A} = +0.03$ and $+0.14$‰ (Nielsen et al., 2018). The isotopically lighter values of this range are likely produced by sediment recycling into the upper mantle, which was concluded to generate enriched MORB reservoirs (Nielsen et al., 2018). Thus, the depleted upper mantle is likely characterized by $\delta^{138/134}Ba_{NIST\ 3104A} \sim +0.14$‰ (Nielsen et al., 2018).

In summary, the Ba isotope composition of subducted slab materials such as marine sediments and AOC can be substantially more variable than the upper mantle. In addition, sediments generally exhibit Ba isotope compositions equal to or lighter than the upper mantle, whereas AOC displays values equal to or heavier than the upper mantle (Fig. 2). Therefore, Ba isotope variations in arc magmas have the potential to fingerprint the source of their excess Ba, which can place constraints on the processes governing mass transfer from the slab to the surface in subduction zones.

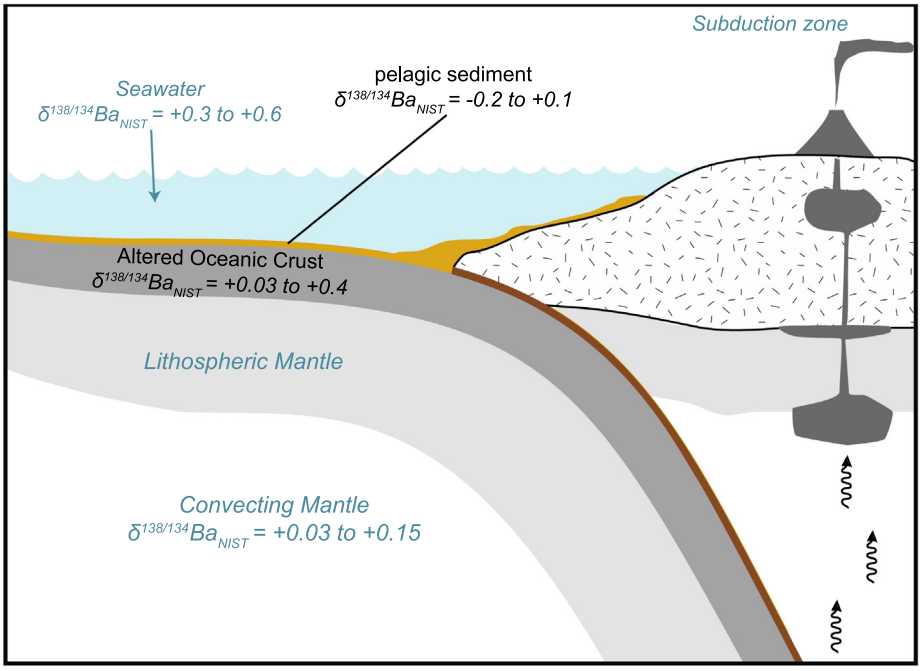

Fig. 2. Summary of the Ba isotope composition ranges for different global reservoirs relevant to subduction zone magmatism. Dark brown area at slab-mantle interface signifies region most likely to supply slab material to arc magmas, which could be composed of sediment, AOC, and subduction erosion material as discreet components and/or mélange.

3. SAMPLES AND METHODS

We have analyzed the Ba isotope compositions of 66 arc magmas from the Aleutian and Ryukyu arcs, supplemented by analysis of 16 back-arc magmas from the Ryukyu arc (Okinawa Trough). The Aleutian magmas analyzed here (see Nielsen et al., 2016) cover the entire length of the arc from ~188°W in the Western Aleutians to ~165°W in the Eastern Aleutians and consist primarily of basalts and basaltic andesites with <56% SiO_2 (Nielsen et al., 2016). The Ryukyu arc magmas also cover the entire length of the arc from S. Kyushu (~31°N) to the S. Ryukyu volcanic front (~24°N) (Shu et al., 2017). The Ryukyu samples also are mostly basalts and basaltic andesites with <56% SiO_2, although three samples from S. Ryukyu are highly evolved. Okinawa Trough samples are also relatively primitive magmas (<56% SiO_2) although five from the S. Okinawa Trough are highly evolved (Shu et al., 2017). All samples have previously been studied for thallium (Tl) isotope compositions and analyzed or reanalyzed for their major and trace element contents, as well as radiogenic Nd, Sr and Pb isotopes (Shinjo et al., 2000; Plank, 2005; Nielsen et al., 2016; Shu et al., 2017). We complement these data with Ba isotope measurements of sediments drilled outboard of both arcs, specifically DSDP Hole 183 and ODP Hole 886C (both Aleutians) and DSDP Holes 294, 295, 296, 442B, 443, and 444 (all Ryukyu) that were also part of the previous Tl isotope studies (Nielsen et al., 2016; Shu et al., 2017).

All sample preparation was conducted in the NIRVANA (Non-traditional Isotope Research for Various Advanced Novel Applications) lab at Woods Hole Oceanographic Institution. Analyses were performed using a Neptune MC-ICP-MS, with instrumental mass bias corrected using a ^{135}Ba–^{136}Ba double spike (Nielsen et al., 2018). Samples were dissolved in 1:1 mixtures of concentrated HF and HNO_3 on a hotplate overnight followed by evaporation and repeated refluxing in concentrated HNO_3 to remove fluorides. Separation of Ba from sample matrix followed methods outlined in previous studies (Horner et al., 2015; Nielsen et al., 2018). Briefly, the method consists of liquid ion exchange chromatography and employs the AG50W-X8 cation exchange resin. About 50 ng of Ba is processed through the column procedure and spiked and equilibrated with an appropriate amount of double spike prior to ion exchange separation. Mass spectrometry follows the methods detailed elsewhere (Horner et al., 2015; Nielsen et al., 2018) where each sample is typically analyzed in quadruplicate. This procedure returns 2SE uncertainties of ~0.02–0.04‰, which is similar to the long-term external 2SD reproducibility of ±0.03‰ that was assessed based on replicate measurements of USGS reference materials (Horner et al., 2015; Nielsen et al., 2018). As in our previous Ba isotope studies, we here report either the 2SE of the four sample analyses or the long-term 2SD of the method, whichever was greater.

4. RESULTS

Magmas from the Central (~179–171°W) and Eastern (~171–163°W) portions of the Aleutian arc exhibit a small, but resolvable Ba isotope variation from $\delta^{138/134}Ba_{NIST\ 3104A} = -0.02‰$ to +0.11‰, whereas the Western Aleutian (west of 179°W) samples display a narrower, but overlap-

Table 1
Ba isotope compositions of magmas from the Aleutian arc.

Sample	SiO_2*	Mg#*	$\delta^{138/134}Ba_{NIST\ 3104A}$	2SD^	n	Ba (μg/g)*
Central and Eastern Aleutians						
Kanaga 514	49.4	0.42	0.08	0.03	4	413
Kanaga 58	56.4	0.49	0.11	0.03	4	552
Kanaga S489	46.9	0.47	0.03	0.03	4	396
Kanaga S508	47.6	0.48	0.04	0.04	3	378
Moffett 18-15A#	49.5	0.46	0.06	0.03	4	370
Moffett 18-15B#	49.2	0.45	−0.02	0.04	4	379
Moffett 2A	49.6	0.52	−0.02	0.05	5	395
Moffett 81 19A	50.3	0.44	0.05	0.04	3	440
Okmok UM-10	51.3	0.64	0.01	0.04	4	206
Okmok UM-21	51.6	0.49	0.03	0.04	4	230
Okmok UM-23	53.3	0.42	0.08	0.04	4	344
Okmok UM-5	52.3	0.46	0.06	0.03	4	332
Westdahl SAR −4	61.5	0.34	0.01	0.03	4	726
Westdahl SAR-11	51.0	0.40	0.09	0.07	5	361
Westdahl SAR-17	48.3	0.39	0.08	0.03	4	395
Westdahl SAR-7	50.5	0.43	0.06	0.03	4	306
Western Aleutians						
tn182_01_001	65.9	0.61	−0.04	0.03	4	301
tn182_03_002	64.0	0.58	0.04	0.03	4	246
tn182_04_003	66.3	0.62	0.05	0.03	4	165
tn182_05_001	55.8	0.63	−0.02	0.03	4	291
tn182_07_002	52.0	0.68	0.01	0.03	4	284
tn182_07_005	64.9	0.63	0.02	0.03	4	256
tn182_07_009	64.3	0.64	0.07	0.03	4	252
tn182_08_003	51.8	0.71	0.03	0.03	4	223
tn182_08_013	51.9	0.70	0.01	0.03	4	243
tn182_08_014	52.1	0.69	0.01	0.03	4	242
tn182_09_001	50.4	0.66	0.04	0.03	4	231
tn182_10_003	58.3	0.45	0.02	0.04	4	443
tn182_10_004	61.1	0.61	0.06	0.03	4	647
tn182_13_001	53.2	0.65	0.01	0.03	4	292
SO201-1b-33-001	69.2	0.66	0.04	0.03	4	117
SO201-1b-35-004	70.2	0.64	0.04	0.03	4	124
SO201-1b-36-003	69.6	0.69	0.00	0.03	4	118

* Major element and Ba concentrations from Plank (2005) and Yogodzinski et al. (2015).
^ The quoted uncertainty represents either the 2SE of the 3–5 sample analyses or the long-term 2SD of the method, whichever is greater.
# These samples have also been published with the name MOF 81-15 (Yogodzinski et al., 2011) and MOF 15 (Kay and Kay, 1994).

ping variation of $\delta^{138/134}Ba_{NIST\ 3104A} = -0.04‰$ to $+0.07‰$ (Table 1). Thus, there is no indication that lavas thought to be strongly influenced by slab melting (Western Aleutians) are systematically different to those that are less so (Central and Eastern Aleutians) (Yogodzinski et al., 1995, 2015). Sediments outboard of the Aleutian arc display roughly similar values to the magmas with DSDP 183 sediment (situated outboard of the Eastern Aleutians) exhibiting values of $\delta^{138/134}Ba_{NIST\ 3104A} = -0.01‰$ to $+0.09‰$ and ODP 886C (situated outboard of the Central Aleutians) varying from $\delta^{138/134}Ba_{NIST\ 3104A} = -0.05‰$ to $+0.11‰$ (Table 2).

Magmas from the Ryukyu arc display similar values to the Aleutian samples with an overall range of $\delta^{138/134}Ba_{NIST\ 3104A} = -0.07‰$ to $+0.09‰$, whereas the Okinawa Trough magmas are characterized by $\delta^{138/134}Ba_{NIST\ 3104A} = -0.06‰$ to $+0.09‰$ (Table 3). Sediments outboard of the S. Ryukyu arc (DSDP 294 and 295) exhibit a small range in Ba isotopes from $\delta^{138/134}Ba_{NIST\ 3104A} = +0.02‰$ to $+0.14‰$, whereas carbonate sediments (DSDP 296) and detrital sediments (DSDP 442B, 443, and 444) outboard of S. Kyushu display values of $\delta^{138/134}Ba_{NIST\ 3104A} = +0.01‰$ to $+0.08‰$ and $\delta^{138/134}Ba_{NIST\ 3104A} = -0.02‰$ to $+0.15‰$, respectively (Table 4). The general range of Ba isotope compositions in all the sediment samples are very similar to those reported for sediments from the oligotrophic (nutrient depleted) South Atlantic (Bridgestock et al., 2018) and various sediment core tops from different oligitrophic regions (Nielsen et al., 2018).

Here we use the trace element concentrations and isotope compositions determined for sediments outboard of the Ryukyu arc and Aleutians to construct weighted average subducted sediment compositions for Northern Ryukyu (DSDP 442B, 443, and 444), Southern Ryukyu (DSDP 294 and 295), the Eastern Aleutians (DSDP 183) and Central Aleutians (ODP 886C) (Tables 2 and 4). It was previously concluded that carbonate sediments drilled at DSDP Site 296 were unlikely to represent a significant part of the subducted sediment package in the Ryukyu arc (Shu et al., 2017). We, therefore, do not plot these along

Table 2
Barium isotope compositions for sediments outboard of the Aleutian arc.

Sample name	Sediment type	Depth (mbsf)	$\delta^{138/134}Ba_{NIST\ 3104A}$ [#]	2SD[^]	n	Ba (μg/g)[*]
DSDP Site 183						
2R-3 52-54 cm	Clay with diatom	6.53	0.04	0.04	4	1012
9R-3 82-84 cm	Clay with diatom	71.83	0.03	0.04	7	802
17R-3 72-74 cm	Diatom ooze	167.73	−0.01	0.03	4	2588
21R-1 129-131 cm	Diatom with clay	202.3	0.05	0.06	2	16,382
Average diatom ooze			*0.04*			*5196*
22R-2 95-97 cm	Silty clay	212.46	0.07	0.03	4	933
24R-3 85-87 cm	Clay	232.86	0.09	0.04	4	680
27H-3 36-38 cm	Silt	260.37	0.03	0.04	4	783
38R-2 68-70 cm	Clay	474.19	0.03	0.04	3	744
Average clay and turbidite			*0.06*			*785*
Average DSDP 183 sediment			**0.05**			**2074**
ODP Site 886C						
1H-4 70-72 cm	Reddish brown clay	5.21	0.04	0.03	3	2801
2H-4 65-67 cm	Light brown spicule clay	11.96	0.06	0.03	6	nd
4H-1 80-82 cm	Light brown diatom ooze	26.61	0.11	0.03	4	2995
5H-1 50-52 cm	Light brown diatom ooze	35.81	0.05	0.04	4	2302
6H-3 120-122 cm	Mn nodule	49.01	−0.05	0.04	3	2497
8H-1 48-50 cm	Dark brown clay	64.29	0.06	0.04	4	593
Average ODP 886C sediment			**0.05**			**3910**

nd - not determined.
[*] Barium concentrations of discreet sediment samples are from Kay and Kay (1988) for DSDP 183 samples and Nielsen et al. (2016) for ODP 886C samples. Average Ba contents for DSDP Site 183 from Plank and Langmuir (1998) and ODP Site 886C from Nielsen et al. (2016). These averages are based on larger sample sets than what was analyzed for Ba isotopes. However, samples analyzed for Ba isotopes represent all the major sedimentary lithologies encountered at each site.
[^] The quoted uncertainty represents either the 2SE of the 2 to 7 sample analyses or the long-term 2SD of the method, whichever is greater.
[#] Average Ba isotope composition for DSDP Site 183 sedimentary units calculated by weighting each sample by its Ba concentration. The two major sediment types at Site 183 were then weighted by their relative thicknesses and Ba concentrations. Average Ba isotope composition of ODP Site 886C was calculated by weighting sediment types by their thicknesses, densities, and Ba concentrations as given in Nielsen et al. (2016).

with other sediment components. However, it is worth noting that the weighted average Ba isotope composition of these carbonates is identical to the other sediments outboard of the Ryukyu arc (Table 4). This result is perhaps expected given that the Ba content of both carbonate and detrital sediments are likely controlled by the abundance of barite, the isotopic composition of which is set by regional oceanographic features, as outlined in Section 2.2. The carbonate-free sediment Ba isotope composition averages presented here were weighted by the same lithological abundance and density data used to reconstruct the average geochemical composition of subducted sediments in these locations (Plank and Langmuir, 1998; Nielsen et al., 2016; Shu et al., 2017). These weighted average sediment compositions are used as best estimates for the composition of the subducted sediments, along both the Aleutian and Ryukyu arcs, in the following discussion.

5. DISCUSSION

5.1. No evidence for Ba isotope effects from assimilation and fractional crystallization

The majority of the samples investigated here are basaltic and contain $< 56\%$ SiO_2 (Nielsen et al., 2016; Shu et al., 2017). However, a few samples are more evolved ($SiO_2 > 60\%$, Fig. 3) and it is possible that their Ba isotope compositions could have been affected by removal of Ba during fractional crystallization (for example from amphibole crystallization (Kay and Kay, 1994)) or Ba addition during crustal assimilation. The highly incompatible nature of Ba suggests that modest degrees of fractional crystallization are unlikely to change the overall Ba budget of a magma. The most SiO_2-rich samples tend to have slightly lower Ba/Th ratios than more primitive magmas from the same region (Fig. 3a). However, none of the samples investigated here are cogenetic, which renders it difficult to assess whether variations in Ba/Th are due to magmatic differentiation and assimilation or simply a function of variable Ba/Th in the source regions of these magmas. For the Western Aleutians it is particularly difficult to assign the variations in SiO_2 to magmatic differentiation as some of these samples may be relatively primitive melts (Yogodzinski et al., 2015). However, the high SiO_2 samples from the Ryukyu Arc, Okinawa Trough, and Central and Eastern Aleutians likely represent more evolved magmas. These samples exhibit Ba isotope compositions that remain within the same range of values as more primitive magmas from the same arc (Fig. 3b). This evidence suggests that even if assimilation or fractional crystallization modified the Ba concentration and/or isotope composition of the magma, these effects appear to either not be associated with any Ba isotope fractionation or have been so minor that they did not induce any systematic changes in the magma Ba isotope compositions. We, therefore, conclude that all magmas studied here are likely to closely resemble the Ba isotope composition imparted during initial melt generation.

Table 3
Ba isotope compositions of magmas from the Ryukyu arc and Okinawa Trough.

Sample	Longitude, deg. N	SiO_2*	Mg#*	$\delta^{138/134}Ba_{NIST\ 3104A}$	2SD^	n	Ba (μg/g)*
Ryukyu arc							
KR-01	31°53′	50.8	0.47	−0.02	0.03	5	196
KR-03	31°53′	50.5	0.48	0.03	0.03	5	153
HOKU8	31°47.6′	54.1	0.57	0.01	0.03	4	276
NK01	31°46.4′	51.5	0.59	0.04	0.04	4	660
HOKU34	31°46.2′	48.8	0.47	0.01	0.03	4	113
HOKU33	31°45.8′	48.1	0.50	0.02	0.03	5	100
HOKU43	31°41.3′	51.4	0.51	0.05	0.03	4	105
HOKU41	31°39.2′	51.5	0.52	−0.02	0.03	4	126
OND	31°14.5′	51.8	0.52	0.04	0.03	4	174
KIM1	31°11′	52.5	0.44	0.03	0.03	4	134
MKR2	30°49′	55.5	0.48	0.05	0.03	5	229
IW03	30°47′	51.1	0.49	0.09	0.04	4	93
KC4	30°27′	54.0	0.50	0.01	0.03	5	178
KUC5	29°58′	55.1	0.44	−0.02	0.03	5	157
NAK13	29°51′	53.4	0.46	0.04	0.03	4	132
SUW13	29°38′	53.1	0.51	0.09	0.03	3	111
SUW14	29°38′	53.8	0.47	0.05	0.03	4	103
AK3	29°27′	54.7	0.50	−0.04	0.03	4	114
YOK4	28°47.5′	52.5	0.49	−0.02	0.02	6	105
TR2	27°52′	50.9	0.47	0.01	0.03	4	38
KB	26°23.175′	50.9	0.69	−0.03	0.03	5	124
OJ-1	26°20.138′	56.2	0.66	0.04	0.03	4	433
6K-569-2	25°14.425′	50.3	0.45	0.03	0.03	4	96
6K-562-8	25°14.174′	50.7	0.47	0.03	0.03	6	93
6K-562-10	25°13.851′	52.05	0.46	−0.07	0.03	4	94
DELP88-5B	25°13.68′	53.1	0.49	0.07	0.03	4	61
RN97-D6A	25°05.31′	75.1	0.12	0.09	0.04	3	220
D3K-460-1	24°57.83′	69.5	0.30	0.07	0.03	4	416
RN07-DR3-1	24°54.537′	55.5	0.48	0.03	0.03	4	181
2K-797-956233	24°51′	67.7	0.27	0.04	0.03	4	349
RN07-DR1-3	24°51.602′	55.5	0.34	0.04	0.03	3	103
2K-866-9651411	24°46′	55.0	0.40	0.03	0.03	4	163
2K-1178-2	24°42.575′	52.2	0.54	0.06	0.03	4	126
Okinawa Trough							
DELP84-D1YK	28°07.3′	50.4	0.55	0.09	0.03	4	76
CB6-22	27°34.61′	49.2	0.61	0.06	0.03	3	75
A6	27°31.33′	51.9	0.54	−0.05	0.03	4	95
A1A	27°24.37′	50.9	0.58	0.05	0.03	4	75
JCD-3	27°01.99′	52.7	0.56	−0.06	0.03	6	118
B1A	27°01.29′	51.7	0.57	−0.01	0.03	5	107
B1B	27°01.29′	52.7	0.55	0.03	0.03	4	109
6K-563-2	25°15.821′	50.5	0.41	0.02	0.03	4	90
JCD-4	25°14.07′	54.7	0.36	0.06	0.03	4	117
2K-1177-4	24°56.977′	50.2	0.49	−0.05	0.03	4	126
6K-559-1	24°56.241′	68.9	0.23	0.00	0.02	7	503
HK02-D5-5	24°54.29′	74.6	0.23	−0.01	0.03	4	512
HK02-D6-4	24°51.97′	53.0	0.49	0.02	0.02	5	140
2K-1176-7	24°51.892′	70.7	0.27	0.01	0.03	4	483
6K-560-7	24°51.544′	71.0	0.25	0.02	0.03	4	499
D3K-459-1	24°48.847′	64.9	0.34	0.01	0.03	4	421

* Major element and Ba concentrations from Shinjo et al. (1999, 2000) and Shu et al. (2017).
^ The quoted uncertainty represents either the 2SE of the 3–7 sample analyses or the long-term 2SD of the method, whichever is greater.

5.2. Barium isotope fractionation during slab mobilization

In this section, we combine new Ba isotope data for magmas and sediments in the Aleutian and Ryukyu arcs (Tables 1–4), with previously determined compositions of the upper mantle and AOC (Nielsen et al., 2018), to perform a general assessment of the partitioning of Ba isotopes within subduction zones. With this dataset, we are able to

Table 4
Ba isotope compositions of sediments outboard of the Ryukyu arc.

Sample name	Sediment type	Depth (mbsf)	$\delta^{138/134}Ba_{NIST\ 3104A}$ [#]	2SD[^]	n	Ba (μg/g)[*]
DSDP sites 294 and 295						
294 1R-1 122–124 cm	Brown silt-rich clay	1.22	0.09	0.04	4	472
294 3R-4 63–65 cm	Dusky brown clay	79.13	0.05	0.04	4	134
294 4R-3 70–72 cm	Dusky brown clay	96.7	0.14	0.04	4	670
294 6R-1 72–74 cm	Red silt-rich clay	106.22	0.07	0.04	4	1622
295 1R-4 74–76 cm	Brown clay	106.24	0.05	0.04	4	330
295 3R-3 80–82 cm	Dusky brown silty clay	142.8	0.06	0.04	4	1290
Average DSDP 294 and 295 sediment			**0.07**			**670**
DSDP site 296						
2R-4 64–66 cm	Nannofossil clay	11.64	0.08	0.04	4	435
5R-3 33–35 cm	Nannofossil clay	38.33	0.04	0.04	4	512
6R-3 106–108 cm	Clay-rich nannofossil ooze	48.56	0.02	0.04	4	388
7R-2 75–77 cm	Clay-rich nannofossil ooze	56.25	0.04	0.03	5	548
8R-4 12–14 cm	Clay-rich nannofossil ooze	68.12	0.03	0.03	8	321
10R-2 74–76 cm	Clay-rich nannofossil ooze	84.74	0.03	0.03	8	348
16R-3 83–85 cm	Nannofossil ooze/chalk	143.33	0.01	0.03	8	276
21R-4 85–87 cm	Nannofossil ooze/chalk	192.35	0.02	0.04	4	1022
24R-3 106–108 cm	Nannofossil ooze/chalk w. radiolarians	219.56	0.04	0.04	4	826
29R-5 96–98 cm	Nannofossil ooze/chalk w. radiolarians	269.96	0.01	0.04	4	870
31R-2 98–100 cm	Clayey nannofossil chalk	284.48	0.14	0.04	4	672
32R-4 65–67 cm	Clayey nannofossil chalk	296.65	0.12	0.04	4	1056
Average DSDP 296 sediment			**0.05**			**677**
DSDP sites 442B, 443, 444						
442B 1R-1 55–57 cm	Grayish clay	268.05	0.05	0.04	4	877
442B 1R-2 77–79 cm	Greenish-gray clay	269.64	0.03	0.04	4	1440
442B 2R-2 83–85 cm	Dark brown zeolitic clay	279.33	0.05	0.04	4	1713
442B 2R-4 50–52 cm	Dark brown zeolitic clay	281.52	0.06	0.04	4	1833
443 1R-2 30–32 cm	Dark-greenish-gray mud	1.8	0.08	0.04	4	646
444 2R-3 68–70 cm	Dark-greenish-gray mud	9.68	0.05	0.04	4	793
444 3R-2 82–84 cm	Dark-greenish-gray mud	17.82	−0.02	0.02	8	676
444 5R-2 30–32 cm	Olive gray mud	36.3	0.04	0.03	4	866
444 5R-4 40–42 cm	Olive gray mud	39.4	−0.02	0.04	4	854
444 7R-1 34–36 cm	Light olive brown mud	53.84	−0.01	0.03	8	439
444 9R-1 46–48 cm	Light olive brown mud	72.96	0.15	0.03	4	2105
Average DSDP sites 442B, 443, 444 sediment			**0.06**			**1170**

[*] Barium concentrations for discreet sediment samples and weighted site averages are from Shu et al. (2017).
[^] The quoted uncertainty represents either the 2SE of the 3–8 sample analyses or the long-term 2SD of the method, whichever is greater.
[#] Average Ba isotope compositions are weighted according to sedimentary lithological thicknesses, densities and Ba concentrations as outlined in Shu et al. (2017).

constrain the Ba isotopic mass balance of almost the entire subduction zone; inputs—sediments, AOC, and the upper mantle—and a significant fraction of the outputs (i.e., the arc magmas). As outlined in section 2.2, the upper mantle varies from $\delta^{138/134}Ba_{NIST\ 3104A} = +0.03 \pm 0.02‰$ for the enriched MORB mantle end-member to $+0.14 \pm 0.02‰$ for the depleted MORB mantle (DMM) end-member. Altered oceanic crust likely possesses compositions no lighter than enriched MORB and possibly as heavy as $\delta^{138/134}Ba_{NIST\ 3104A} \sim +0.4‰$ (Nielsen et al., 2018). The subducted sediment packages in the four drill sites from the two arcs investigated (DSDP 183 and ODP 886C in front of the Aleutians and DSDP 294/295 and DSDP 442B, 443 and 444 in front of the Ryukyu arc) all have weighted average $\delta^{138/134}Ba_{NIST\ 3104A}$ between +0.05 and +0.08‰ (Tables 2 and 4). That is, all bulk subduction zone inputs in the Aleutian and Ryukyu arcs display $\delta^{138/134}Ba_{NIST\ 3104A} > 0.03‰$. In contrast, at least 40% of the arc magmas display Ba isotope compositions lighter than any of the principal inputs by up to ~0.10‰ (Fig. 4). In addition, there is no indication of a significant systematic spatial trend in Ba isotopes along either arc (Fig. 4), suggesting that there is a small-but-systematic Ba isotope difference between bulk inputs (the mantle, sediments, and AOC) to and outputs (arc lavas) from these two arcs. The only potential input component that we have not accounted for in this study are serpentinites, which are mantle rocks that have reacted extensively with and had water added. These rocks are often inferred to account for a significant portion of the water that is thought to drive much of the arc volcanism associated with subduction zones (Worzewski et al., 2011; Deschamps et al., 2013). However, serpentinites typically have very low Ba concentrations because the mantle rock protoliths are Ba-poor and the hydrothermal reactions that cause serpentinization does not add significant Ba (Kodolanyi et al., 2012; Debret et al., 2013; Deschamps et al., 2013). As such, it is unlikely that fluids released from serpentinites would contain

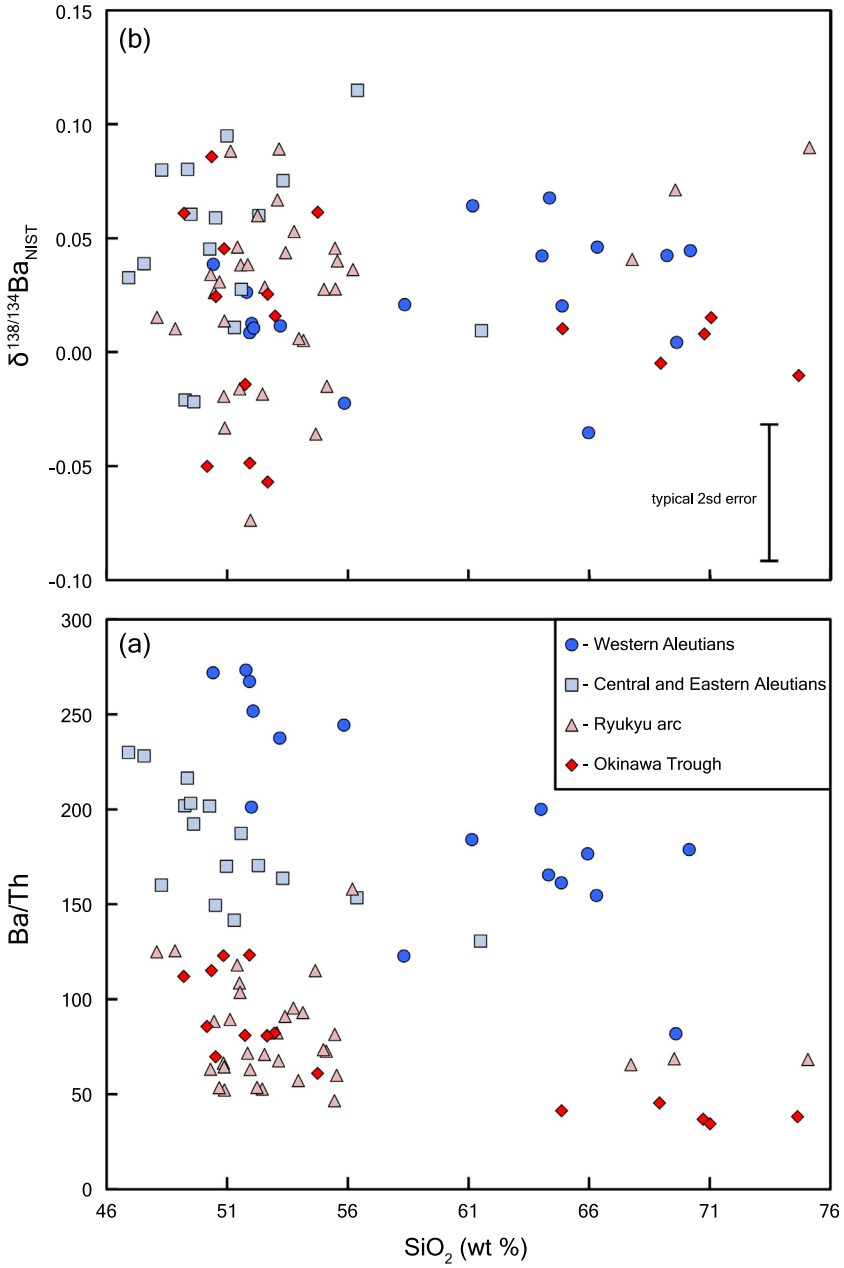

Fig. 3. Barium isotope and Ba/Th ratios plotted against SiO_2 concentrations for magmas from the Aleutian arc and the Ryukyu arc-Okinawa Trough. It is evident that fractional crystallization and assimilation processes that occur as SiO_2 increases do not cause a discernible change in Ba isotopes. However, Ba/Th ratios are generally lower in high-SiO_2 samples suggesting that the Ba budget of magmas are not entirely unperturbed by fractional crystallization and assimilation.

sufficient Ba to perturb the Ba budget of subduction fluids and Ba enrichments in arcs are generally thought to arise primarily from sediments (Plank and Langmuir, 1993).

There are several mechanisms that can potentially explain the Ba isotopic offset between the arc inputs and the magmas.

(1) One of the arc inputs (e.g. sediments or AOC) contains a component that is characterized by fractionated Ba isotopes and preferentially released from the slab either in the forearc (Solomon and Kastner, 2012) or as the main supplier of Ba to arc magmatism. This component could, for example, be barites that might dissolve during early stages of subduction in the forearc (Solomon and Kastner, 2012). If this was the case, then the dissolved barites should be systematically heavy, thus leaving the residual sediments lighter than bulk sediments. The opposite situation, where barites are isotopically lighter than bulk sediment, could be imagined if barites were preferentially mobilized at the slab-mantle interface and thus were the main source of the isotopically light Ba in arc magmas. However, if either of these explanations were correct, then we would expect to observe systematically different Ba

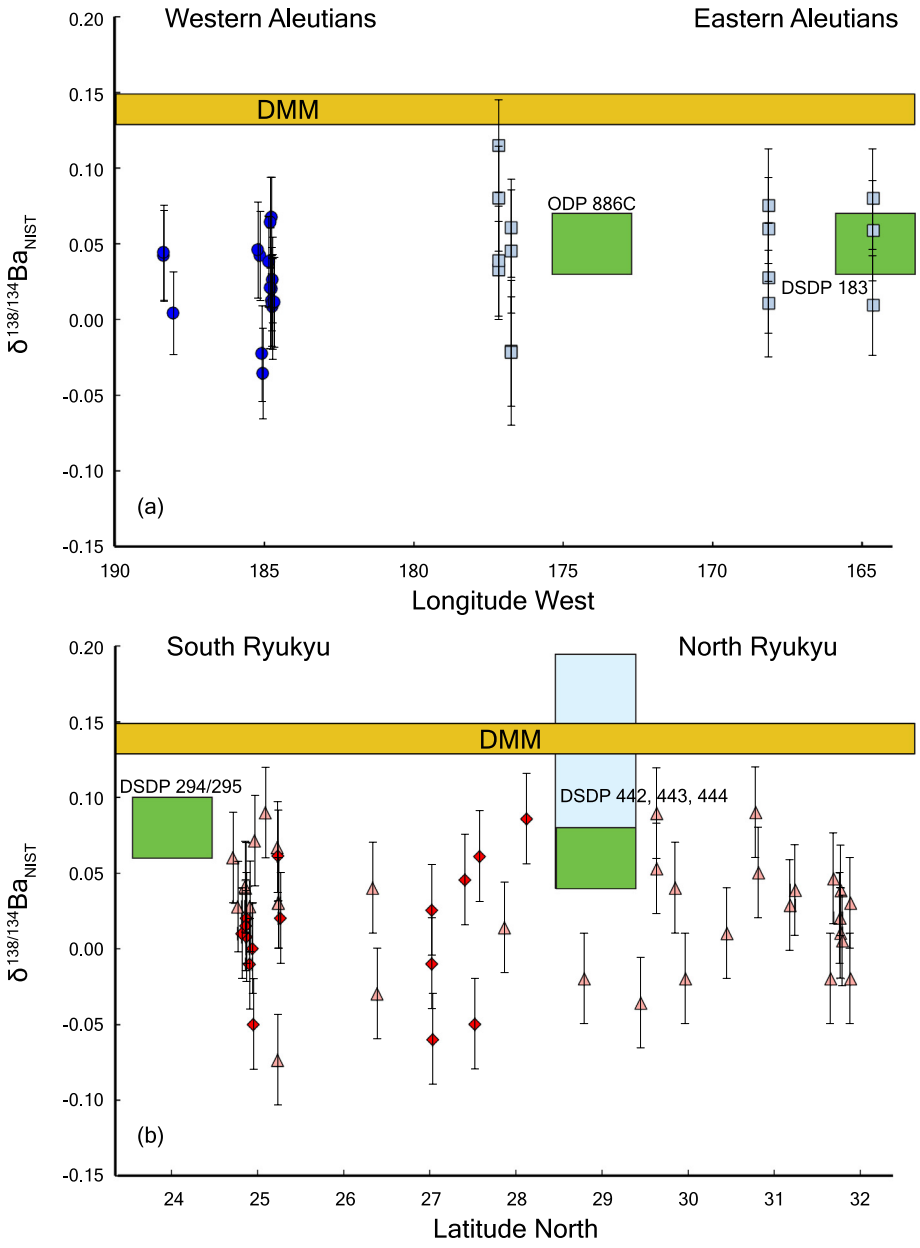

Fig. 4. Barium isotope variation along strike of (a) the Aleutian arc and (b) the Ryukyu arc-Okinawa Trough. Also shown are weighted average Ba isotope compositions and approximate subduction location of sediments (green squares) and AOC (light blue square). The composition of the depleted MORB mantle (DMM) is also shown as a yellow rectangle. Symbol shapes and colors are the same as in Fig. 3. (For interpretation of the references to colour in this figure legend, the reader is referred to the web version of this article.)

isotope compositions in sediments with the highest Ba concentrations because Ba in these samples almost exclusively resides in barite. However, there is no correlation between Ba isotopes and concentrations in discreet sediment samples (Tables 2 and 4), which implies that barites are not characterized by Ba isotope compositions significantly different to bulk sediments. This inference is in agreement with Ba isotope compositions of sedimentary barites that are typically between $\delta^{138/134}Ba_{NIST\ 3104A} \sim 0$–$0.1$ (Bridgestock et al., 2018; Nielsen et al., 2018). Average upper continental crust is also characterized by $\delta^{138/134}Ba_{NIST\ 3104A} \sim 0$ (Nan et al., 2018), such that residual sediments after barite dissolution should not be characterized by Ba isotope compositions as light as those observed in the Aleutian and Ryukyu arc magmas. Thus, preferential mobilization of barite during progressive forearc sediment burial (Solomon and Kastner, 2012) or at the slab-mantle interface is unlikely to explain the light Ba isotope values seen in arc magmas.

(2) It is possible that an arc input exists that we have not characterized in our data set, which displays light Ba isotope compositions. One such input could, for example, be forearc crustal materials added to the top of the slab via forearc subduction erosion (von Huene et al., 2004), which

has been suggested as an important process in the Aleutians (e.g. Jicha and Kay, 2018). However, since both the mantle and continental crust are characterized by Ba isotope compositions around or slightly heavier than $\delta^{138/134}Ba_{NIST\ 3104A} \sim 0$ (Nan et al., 2018; Nielsen et al., 2018) there is no reason why forearc crustal materials should be characterized by lighter Ba isotope compositions.

Another possibility is the presence of hydrothermal sediments at the crust-sediment interface that can contain several weight % Ba in the form of barite (Plank and Langmuir, 1998). Some hydrothermally precipitated barites do exhibit Ba isotope compositions almost as light as the lightest values observed for magmas in the Aleutian and Ryukyu arcs (Crockford et al., 2019), suggesting that hydrothermal sediments could be a contributing source to this signature. However, hydrothermal sediments also contain high Pb concentrations with unradiogenic $^{207}Pb/^{204}Pb$ isotope ratios and strong negative Ce anomalies (Plank and Langmuir, 1998), that are not generally observed in the arc magmas with light Ba isotope compositions. Hence, although hydrothermal barites remain a potential source of isotopically light Ba to arc magmas, current evidence does not strongly support this link. However, targeted Ba isotope analyses of hydrothermal sediments previously identified outboard of some arcs like Tonga (Plank and Langmuir, 1998), would help test if there is a clear link between light Ba isotope compositions in arc magmas and hydrothermal sediment subduction.

(3) Since the majority of Ba in arc magmas is sourced from the subducted slab (Kay, 1980; Plank and Langmuir, 1993), there is a small Ba isotope fractionation associated with mobilization of Ba from the subducted slab. Given the very small isotopic contrast between sediment and AOC in the two subduction zones investigated here, it is not immediately evident what specific process is causing this Ba isotope fractionation. However, stable isotope ratios of elements like U, Mo, Fe, Zn and B have also been interpreted to fractionate during progressive mobilization of slab material, primarily through fluids (Ishikawa and Nakamura, 1994; Wunder et al., 2005; Freymuth et al., 2015; Debret et al., 2016; König et al., 2016; Pons et al., 2016; Freymuth et al., 2019). As such, it is possible that similar processes are controlling the small Ba isotope fractionation observed in Aleutian and Ryukyu magmas. For Fe and Zn isotopes, these processes have been observed *in situ* in obducted oceanic lithosphere. However, it is unclear the extent to which such processes are capable of perturbing the Zn and Fe budgets of the entire subduction cycle (Foden et al., 2018; Huang et al., 2018) and, thus, arc lavas. In contrast, the U, Mo, B and Ba isotope compositions of arc lavas implicate a fractionation processes that perturbs the overall budgets of these elements. However, the exact location(s) of the isotope fractionation as well as the physical process(es) by which these occur are likely different. This is illustrated by the fact that isotope fractionation factors ($\Delta_{fluid/melt\text{-}residue}$) are both negative (Ba, U) and positive (Mo, B). Further, isotopic effects due to different redox states (Freymuth et al., 2019) and coordination number (Wunder et al., 2005) have been suggested to control these isotope fractionation factors. For Ba, the redox state is unlikely to play a significant role, given that Ba does not have any notable redox chemistry. Coordination chemistry, on the other hand, could play a role for Ba isotope fractionation, because the primary host of Ba in subducted slabs is phengite (Zack et al., 2001; Shu et al., 2019) in which cations are tetrahedrally coordinated. This coordination number is lower than the eight-fold coordination of aqueous Ba at Earth surface conditions (Persson et al., 1995), which would potentially produce lighter Ba isotopic compositions in the fluid relative to the solid. However, the coordination chemistry Ba in aqueous subduction fluids is currently unknown and such a process remains speculative.

We can further investigate the possible sources of Ba in the two arcs by comparing Ba isotopes and Rb/Ba ratios of the different arc inputs with those in the arc magmas (Fig. 5). The Rb/Ba ratio has been found to be invariant in the upper mantle (Hofmann and White, 1983) and the most recent compilation of MORB data revealed $Rb/Ba = 0.092 \pm 0.004$ (Gale et al., 2013). This invariance strongly implies that these two elements are not fractionated during mantle melting. However, Rb/Ba ratios are highly variable in different slab components, with most subducted sediment packages exhibiting average $Rb/Ba < 0.1$ (Plank and Langmuir, 1998). In contrast, average AOC sections are always characterized by $Rb/Ba > 0.35$ (Staudigel et al., 1996; Bach et al., 2003; Kelley et al., 2003) due to the strong deposition of Rb from seawater during low temperature hydrothermal alteration of the extrusive part of the oceanic crust (Hart, 1969). Experimental data for possible slab components derived either from pure sediment (as melts), AOC (as fluids or fluid-rich melts) or mélange (as melts) all display little fractionation of Rb/Ba relative to the bulk starting composition (Johnson and Plank, 1999; Kessel et al., 2005; Hermann and Rubatto, 2009; Carter et al., 2015; Cruz-Uribe et al., 2018), possibly because both elements are controlled primarily by phengite in the residue. Phengite is ubiquitous in metamorphosed subducted slab materials and strongly incorporates both Ba and Rb (Zack et al., 2001; Shu et al., 2019). Therefore, any residual phengite will buffer the Rb/Ba ratio of melts and fluids released from the slab, which ensures relatively limited Rb/Ba fractionation during slab mobilization. Phengite is likely to be stable at pressures up to ~ 3 GPa and at temperatures to 1000 °C in subducted oceanic crust (Schmidt and Poli, 1998) whereas the stability range in mélanges appears less certain. Notably, mélange melts generated at 2.5 GPa reveal significantly lower Ba/Th ratios than melts at 1.5 GPa (Cruz-Uribe et al., 2018), perhaps indicating phengite remaining in the residue at higher pressures. Therefore, residual phengite might render Rb/Ba ratios in melts similar to bulk slab components regardless of the arc lava generation model. Given these constraints, it follows from Fig. 5 that almost all Ba across the Aleutian arc is sourced from sediments with only very minor Ba coming from AOC, which is a point that has previously been made for Aleutian magmas (Kay and Kay, 1994; Yogodzinski et al., 2017). On the other hand, the Ryukyu arc exhibits a clear influence from sediments as well as AOC (Fig. 5), which is also consistent with previous work based primarily on Pb isotopes (Shinjo et al., 2000).

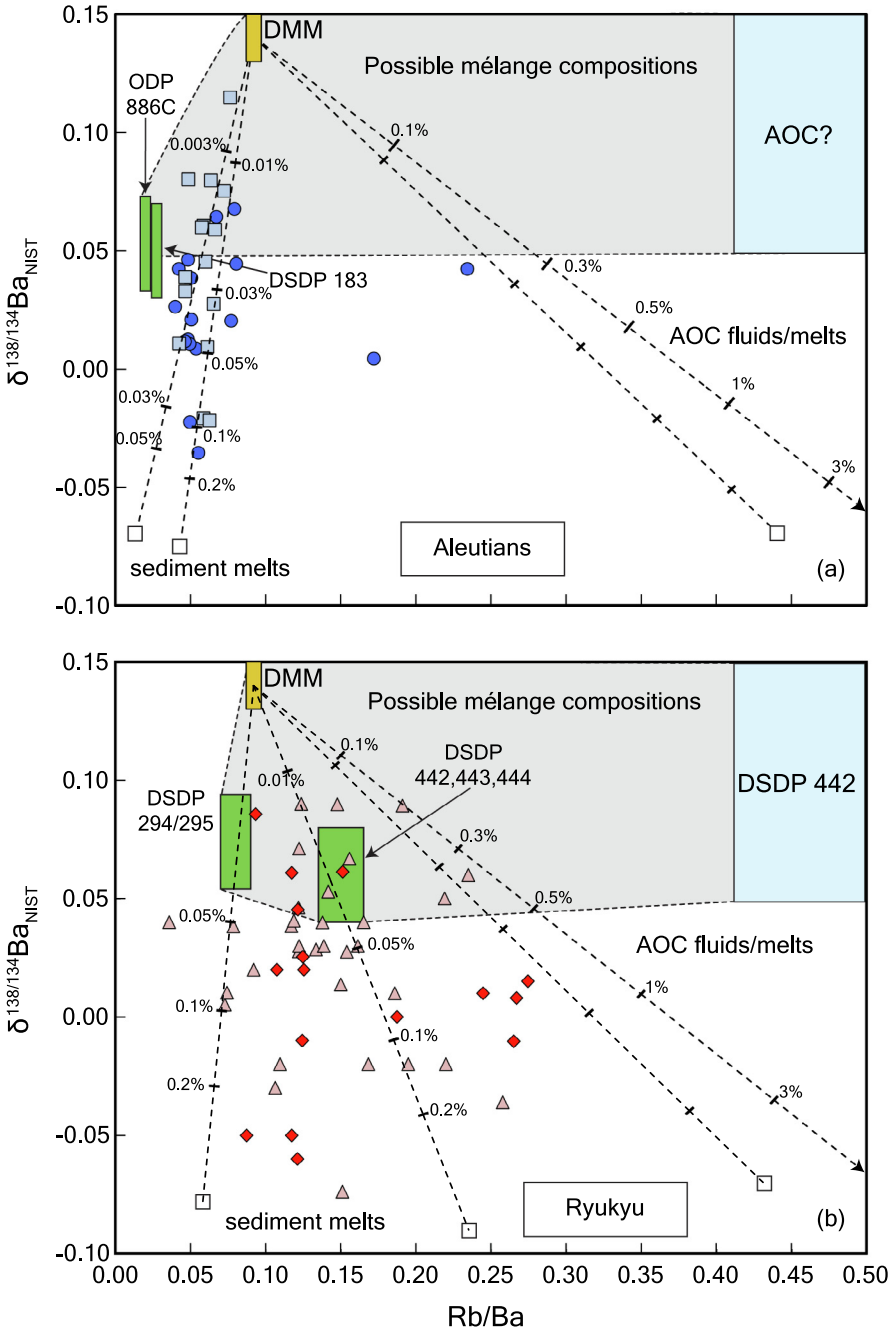

Fig. 5. Barium isotope compositions plotted against Rb/Ba ratios in (a) Aleutian and (b) Ryukyu arc-Okinawa Trough magmas. Also shown are the compositions of the DMM (yellow), subducting sediments (green) and AOC (light blue). Note that no AOC samples are available for the Aleutians and, therefore, the same field as the Ryukyu arc has been assumed. Mixing fields that cover the possible composition of mélanges in each arc have also been indicated in grey with dashed outlines. Symbol shapes and colors for arc magmas are the same as in Fig. 3. Dashed mixing lines between DMM (Workman and Hart, 2005) and potential sediment melts and between DMM and AOC fluids/melts were calculated assuming a fluid/melt fraction of 20% and experimentally derived partition coefficients for Rb and Ba that range between $D_{Ba}/D_{Rb} = 0.6–1.5$ for sediment melts and $D_{Ba}/D_{Rb} = 0.2–2$ for AOC fluids/melts (Kessel et al., 2005; Hermann and Rubatto, 2009; Carter et al., 2015). Ba isotopic fractionation factors of $\Delta^{138/134}Ba_{melt/residue} \sim -0.12$ to $-0.15‰$ were inferred in order to encompass all arc magma data. Tick marks indicate fraction by weight of sediment melt and AOC fluid/melt added to a mantle wedge source region. The two AOC mixing lines have identical tick marks. Sediment melts can fractionate Rb/Ba in both directions depending primarily on temperature (Hermann and Rubatto, 2009) with lowest Rb/Ba ratios resulting from T = 750–800 °C and highest values for T = 900–1050 °C. Here, we show the highest and lowest possible Rb/Ba ratios produced from the sediments in both arcs. Fluids and melts from AOC mostly display higher Rb/Ba than the starting composition (Kessel et al., 2005; Carter et al., 2015), but at T > 1000 °C small fractionations towards lower Rb/Ba (i.e. $D_{Ba}/D_{Rb} > 1$) are possible (Kessel et al., 2005; Carter et al., 2015). Again we show mixing lines for the highest and lowest possible Rb/Ba ratios produced from AOC using all the available experimental data. (For interpretation of the references to colour in this figure legend, the reader is referred to the web version of this article.)

In the Ryukyu arc, it can further be seen that the Ba isotope fractionation is independent of Rb/Ba, with light Ba isotope compositions observed both at low and high Rb/Ba (Fig. 5). If arc melting is initiated via the metasomatised mantle melting process (Fig. 1a) where sediment melts and AOC fluids form two distinct end-members, then the Ba isotope data in the Ryukyu arc would imply that the observed Ba isotope fractionation process occurs both during ocean crust dehydration and sediment melting. Alternatively, if mélange melting is the principle arc melt generation process (Fig. 1b), then Ba isotope fractionation only occurs during the mélange melting/dehydration process. In this interpretation, the mélange at the top of the slab is likely to exhibit a substantial range of Rb/Ba due to the variable mixing proportions of AOC, sediment and mantle, which in turn is inherited by the arc magmas. However, because sediments and AOC, within uncertainty, display identical $\delta^{138/134}Ba_{NIST\ 3104A}$ in the Ryukyu arc, it is not possible to distinguish between a mélange or metasomatised mantle origin using Ba isotopes in this location.

Despite being unable to resolve the relative proportions of sediment melts, AOC fluids, and mélange melts in the Aleutian or Ryukyu arcs, we contend that Ba isotopes may be useful tracers of these sources in other arcs. The utility of Ba isotopes to differentiate these sources depends on the isotopic contrast between sediments and AOC. Due to ocean circulation sedimentary barites deposited in the Southern Ocean and northwest Pacific waters, where strong ocean upwelling renders surface seawater light in terms of Ba isotopes, should also exhibit light Ba isotope compositions. Thus, we anticipate that arcs in these regions—such as the South Sandwich and Kamchatka arcs—will be amenable to Ba-isotopic apportionment of sediment melts, AOC fluids and mélange melts.

5.3. Evidence for AOC contributions

The high Rb/Ba ratios exhibited by some Ryukyu arc magmas require that AOC contributes significantly to the slab component in the Ryukyu arc and Okinawa Trough (Fig. 5). Using the same reasoning, it could be argued that magmas from the Aleutian arc appear to contain a very minimal component derived from AOC. However, this inference is in contradiction to several studies that found Aleutian arc magmas contain a significant component derived from AOC either as a melt derived directly from eclogitized oceanic crust as has been suggested to be a prominent process in the Western Aleutians (Kay, 1978; Yogodzinski et al., 2001, 2015), as eclogitized subducted eroded material from the forearc particularly when the arc migrates (Jicha and Kay, 2018), or as fluids directly from AOC (Miller et al., 1994). On the other hand, the apparent dominance of the sediment component for Ba in the Aleutian magmas could be related to the very high Ba concentrations observed in the subducting sediments outboard of the Aleutian arc (Plank and Langmuir, 1998; Nielsen et al., 2016), which would produce low Rb/Ba in magmas even with very minor sediment addition. Alternatively, it is possible that the eclogite melt component is derived almost exclusively from relatively unaltered oceanic crust characterized by Rb/Ba ratios almost identical to the mantle value of Rb/Ba = 0.092, although a previous investigation found that Western Aleutian slab melts must be generated from hydrated oceanic crust (Yogodzinski et al., 2017). Unaltered oceanic crust has also been suggested as the ultimate source of isotopically fractionated Mo and U in the Mariana and Izu arcs, respectively (Freymuth et al., 2015, 2019). But for Ba this cannot generally be the case as the high Rb/Ba ratios in Ryukyu arc lavas with light Ba isotope compositions (Fig. 5) preclude unaltered oceanic crust as the primary source of Ba there.

As with the Ryukyu arc, it is difficult to further determine the relative importance of AOC and sediment in the Aleutians using Ba isotopes alone since the range of variation between the inputs is relatively narrow (Fig. 4). The only significant difference between the Ba isotope ranges observed in the Aleutians and the Ryukyu arc is the one isotopically heavy sample ($^{138/134}Ba_{NIST\ 3104A} = +0.11‰$) found in the Central Aleutians (Fig. 4). Given that this sample displays more radiogenic Pb isotopic compositions than other magmas from the Central Aleutians (Nielsen et al., 2016), this sample cannot have Ba primarily sourced from the DMM. Instead, it appears more likely that an isotopically heavy slab component ($\delta^{138/134}Ba_{NIST\ 3104A} > 0.25‰$) also plays a role in this portion of the Aleutians.

Such a component would probably originate from AOC (Fig. 6), but since there has never been an AOC section recovered in the vicinity of the Aleutians it is not possible to directly constrain the radiogenic Pb or stable Ba isotope systematics of such a component. If we assume that the Ba isotope composition of AOC subducting at the Aleutians is $\delta^{138/134}Ba_{NIST\ 3104A} > 0.25‰$, which is within the range of observed values in other sections of AOC (Nielsen et al., 2018), and infer reasonable Pb isotope values for AOC based on regional unaltered MORB compositions (Hegner and Tatsumoto, 1987) and the assumption that AOC is characterized by more radiogenic $^{206}Pb/^{204}Pb$ than unaltered MORB (Hauff et al., 2003), then it is possible to produce the range of Ba and Pb isotope compositions determined in the Central and Eastern Aleutian magmas with mixtures of AOC and sediment in which the mass fraction of AOC is substantially larger than the sediments (Fig. 6). This is the case for both mixing calculations in which sediment melts and AOC fluids are mixed with the mantle wedge (Fig. 6a) and when mélange melting is inferred (Fig. 6b). For example, Rb/Ba ratios < 0.08 in the Aleutian magmas are reproduced in mélange compositions even if the mass ratio between AOC and sediment is as high as 16 for pelagic sediment and 7 for detrital sediment (Fig. 6b) and when the mass ratio between AOC fluids and sediment melts are as high as 3 (not shown). In other words, the Ba budget of the arc magmas will be entirely dominated by sediments even if there is substantially more AOC material by mass in the slab component. Some minor fractionation of Rb/Ba towards lower values is possible during any mode of slab material mobilization (Carter et al., 2015; Cruz-Uribe et al., 2018; Hermann and Rubatto, 2009; Johnson and Plank, 1999; Kessel et al., 2005), which could allow for an even larger AOC component in the Aleutian magmas. These calculations highlight

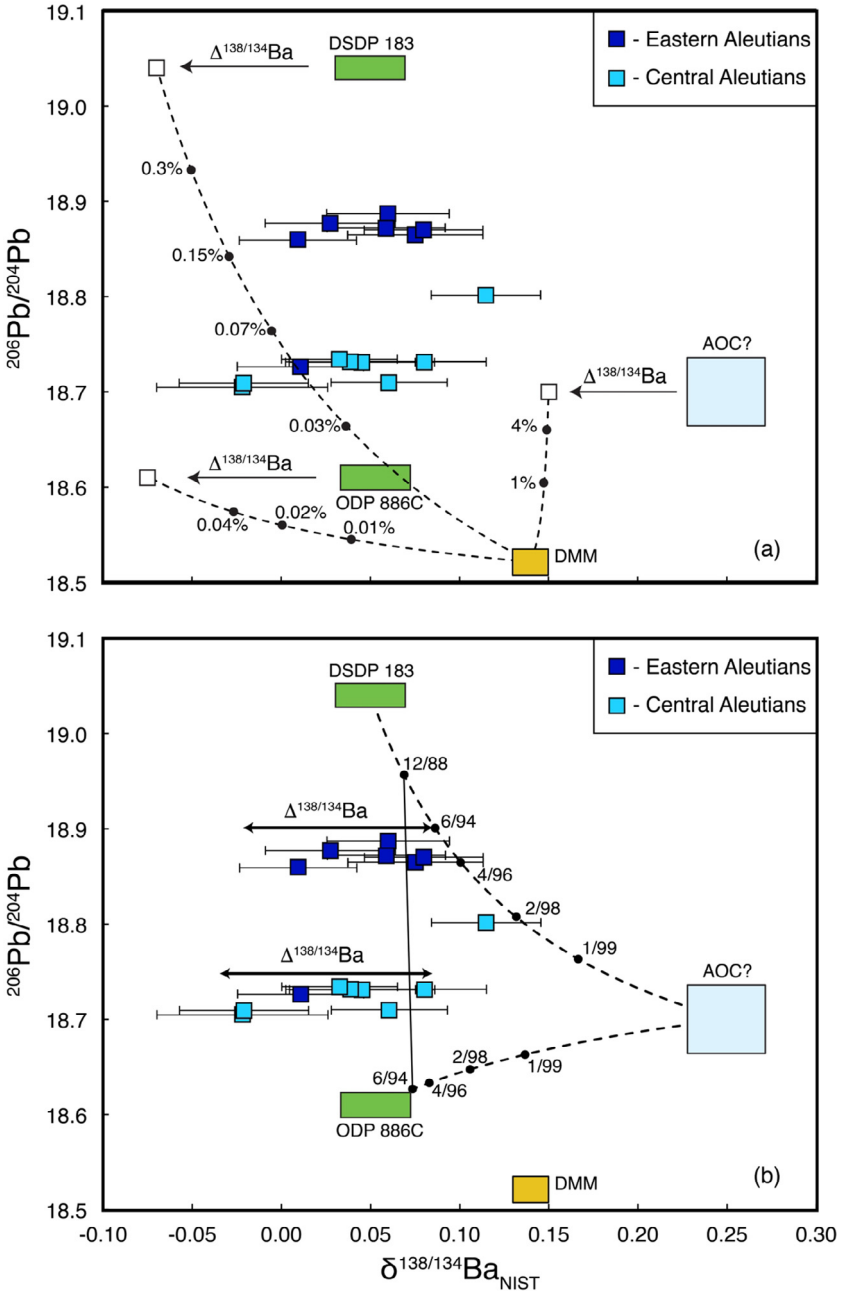

Fig. 6. Ba isotope compositions plotted against $^{206}Pb/^{204}Pb$ isotope ratios in Central and Eastern Aleutian magmas. Western Aleutian samples not shown as these are likely influenced by slab melting and may also contain a different sediment component than the rest of the Aleutian arc. Also shown are fields for subducting sediments (green), DMM (yellow), and a putative field for AOC. The estimated Pb and Ba isotope compositions of the AOC field are based on the requirement that some magmas in the Aleutians exhibit $\delta^{138/134}Ba_{NIST\ 3104A}$ close to +0.1‰, Ba isotopic compositions in AOC sections elsewhere (Nielsen et al., 2018) and the fact that AOC exhibits more radiogenic $^{206}Pb/^{204}Pb$ ratios (Hauff et al., 2003) than regional unaltered MORB (Hegner and Tatsumoto, 1987). The size of the AOC field is not a reflection of how accurately it is constrained. In (a) the same mixing lines between DMM and sediment melts and AOC fluids/melts as in Fig. 5 are shown. Partition coefficients for Ba during sediment melts and AOC fluids are the same as in Fig. 5, whereas no reliable Pb partition coefficients were determined due to issues with Pb contamination during experiments (Hermann and Rubatto, 2009). Therefore, we have estimated melt/residue partition coefficient of $D_{Pb} = 5$, which is similar to that of Sr (Hermann and Rubatto, 2009). Arrows denote the same Ba isotope fractionation as that required Fig. 5, except that the AOC fluid/melt is only fractionated by 0.1‰ relative to bulk AOC. In (b) dashed lines denote bulk mixing between AOC and sediments and the field produced between these three components indicate possible mélange compositions. Tick marks refer to relative proportions of sediment and AOC along the mixing trajectory. Connecting line between 12% DSDP 183 sediments and 6% ODP 886C sediments indicate the point at which bulk Rb/Ba ratios reach the range of values recorded in Aleutian magmas. Larger amounts of AOC produce Rb/Ba significantly higher than values recorded in Aleutian magmas. Bold arrows indicate the likely amount of Ba isotope fractionation needed during slab Ba mobilization processes to account for light Ba isotope compositions. (For interpretation of the references to colour in this figure legend, the reader is referred to the web version of this article.)

that even though Rb/Ba ratios (Fig. 6), thallium (Tl) isotope, and radiogenic Pb isotope data (Nielsen et al., 2016) suggest that these parameters are largely dominated by sedimentary components, it is still possible that an AOC component constitutes a larger proportion, by mass, of the overall slab material present in Eastern and Central Aleutian magmas than sediments do.

6. CONCLUSIONS AND OUTLOOK

We present the first Ba isotope investigations of two subduction zones, the Aleutians and the Ryukyu arc, in which we characterize Ba isotope compositions of the principal slab inputs (sediments and AOC) and the magma outputs erupted at the surface. In both arcs, slab inputs display very narrow ranges in Ba isotope compositions with values of $\delta^{138/134}Ba_{NIST\ 3104A} \sim +0.05‰$ to $+0.08‰$ (Fig. 4). However, $\delta^{138/134}Ba_{NIST\ 3104A}$ of magmas in both arcs extend to values below any of the slab inputs or the DMM. We show that Ba isotope fractionation during fractional crystallization and assimilation is unlikely to explain these values. We also argue that neither barite dissolution in the forearc, subduction erosion processes, or basal hydrothermal barite sediments are likely to explain the light Ba isotope compositions. Instead, these data most likely require that Ba mobilization from the slab produces a small negative isotope fractionation of $\Delta^{138/134}Ba_{melt/residue} \leq -0.15‰$. High Rb/Ba ratios found in many Ryukyu arc and Okinawa Trough magmas provide evidence that Ba from AOC must be a significant slab component in this arc, whereas almost uniformly low Rb/Ba in Aleutian magmas suggest that sedimentary Ba is the dominant source of Ba there. Some heavier $\delta^{138/134}Ba_{NIST\ 3104A}$ values in the Central and Eastern Aleutians also imply that AOC must be a significant component (by mass) in the Aleutian magmas even if the radiogenic Pb and stable Tl and Ba isotope compositions in this portion of the Aleutians imply that sediments impart a strong control on these isotope systems.

The narrow Ba isotope range in slab inputs and erupted magma outputs makes both the Aleutian and Ryukyu arcs ideal locations to investigate Ba isotope fractionation processes during subduction processes. Though resolvable, these internal Ba isotope variations are small. This result better positions subsequent studies to utilize Ba isotopes for the purpose of tracing fluid sources in arcs, which should depend on the Ba source(s) and not internal processes that could fractionate Ba isotopes. With these Ba isotope fractionation effects quantified, we are better positioned to utilize Ba isotopes to test the two end-member slab mobilization models that have been proposed to account for subduction zone melt generation (Fig. 1). As discussed in Section 2.2 there are significant Ba isotope variations in other regions of the ocean that are likely to be imparted into subducting sediments and AOC. For example, sediments subducted in the South Sandwich arc between South America and Antarctica should exhibit $\delta^{138/134}Ba_{NIST\ 3104A} \sim -0.2‰$ to $-0.1‰$, which is much lighter than any likely component from AOC or the mantle. Similarly, sediments deposited outboard of the Kamchatka arc might be isotopically light due to upwelling in this region (Talley, 2013). These configurations of Ba isotope inputs should be much more conducive to assessing if Ba enrichments in arc magmas are produced by AOC fluids, sediment melts, or mélange melts/fluids and future studies at these localities are important in furthering our understanding of Ba cycling and the processes responsible for melt generation in arcs.

Declaration of Competing Interest

The authors declare that they have no known competing financial interests or personal relationships that could have appeared to influence the work reported in this paper.

ACKNOWLEDGEMENTS

This study was funded by grant # NSF EAR 1829546 to SGN and TJH. We thank Heye Freymuth and two anonymous reviewers for their helpful comments that allowed us to improve the manuscript. we also thank Baptiste Debret for comments on an earlier version of this manuscript. Fang Huang is acknowledged for efficient editorial handling.

REFERENCES

Bach W., Peucker-Ehrenbrink B., Hart S. R. and Blusztajn J. S. (2003) Geochemistry of hydrothermally altered oceanic crust: DSDP/ODP Hole 504B - Implications for seawater-crust exchange budgets and Sr- and Pb-isotopic evolution of the mantle. *Geochem. Geophys. Geosyst.* **4**, art. no. 8904.

Bridgestock L., Hsieh Y. T., Porcelli D., Homoky W. B., Bryan A. and Henderson G. M. (2018) Controls on the barium isotope compositions of marine sediments. *Earth Planet. Sci. Lett.* **481**, 101–110.

Carter L. B., Skora S., Blundy J. D., De Hoog J. C. M. and Elliott T. (2015) An experimental study of trace element fluxes from subducted oceanic crust. *J. Petrol.* **56**, 1585–1605.

Chan L. H., Drummond D., Edmond J. M. and Grant B. (1977) On the barium data from the Atlantic GEOSECS expedition. *Deep Sea Res.* **24**, 613–649.

Codillo E. A., Le Roux V. and Marschall H. R. (2018) Arc-like magmas generated by mélange-peridotite interaction in the mantle wedge. *Nat Commun* **9**, 2864.

Crockford P. W., Wing B. A., Paytan A., Hodgskiss M. S. W., Bitterwolf K. K., Hayles J. A., Middleton J., Ahm A. C., Johnston D. T., Caxito F., Uhlein G., Halverson G. P., Eickmann B., Torres M. and Horner T. J. (2019) Barium-isotopic constraints on the origin of post-Marinoan barites. *Earth Planet. Sci. Lett.* **519**, 234–244.

Cruz-Uribe A. M., Marschall H., Gaetani G. A. and Le Roux V. (2018) Generation of alkaline magmas in subduction zones by melting of mélange diapirs. *Geology* **46**, 343–346.

Debret B., Andreani M., Godard M., Nicollet C., Schwartz S. and Lafay R. (2013) Trace element behavior during serpentinization/de-serpentinization of an eclogitized oceanic lithosphere: A LA-ICPMS study of the Lanzo ultramafic massif (Western Alps). *Chem. Geol.* **357**, 117–133.

Debret B., Millet M.-A., Pons M.-L., Bouilhol P., Inglis E. and Williams H. (2016) Isotopic evidence for iron mobility during subduction. *Geology* **44**, 215–218.

Dehairs F., Chesselet R. and Jedwab J. (1980) Discrete suspended particles of barite and the barium cycle in the open ocean. *Earth Planet. Sci. Lett.* **49**, 528–550.

Deschamps F., Godard M., Guillot S. and Hattori K. (2013) Geochemistry of subduction zone serpentinites: A review. *Lithos* **178**, 96–127.

Eagle M., Paytan A., Arrigo K. R., van Dijken G. and Murray R. W. (2003) A comparison between excess barium and barite as indicators of carbon export. *Paleoceanography* **18**.

Elliott T. (2003) Geochemical tracers of the slab. In *Geophysical Monograph* (ed. J. Eiler). American Geophysical Union, pp. 23–45.

Elliott T., Plank T., Zindler A., White W. and Bourdon B. (1997) Element transport from slab to volcanic front at the Mariana arc. *J. Geophys. Res.-Solid Earth* **102**, 14991–15019.

Foden J., Sossi P. A. and Nebel O. (2018) Controls on the iron isotopic composition of global arc magmas. *Earth Planet. Sci. Lett.* **494**, 190–201.

Freymuth H., Andersen M. B. and Elliott T. (2019) Uranium isotope fractionation during slab dehydration beneath the Izu arc. *Earth Planet. Sci. Lett.* **522**, 244–254.

Freymuth H., Vils F., Willbold M., Taylor R. N. and Elliott T. (2015) Molybdenum mobility and isotopic fractionation during subduction at the Mariana arc. *Earth Planet. Sci. Lett.* **432**, 176–186.

Gale A., Dalton C. A., Langmuir C. H., Su Y. J. and Schilling J. G. (2013) The mean composition of ocean ridge basalts. *Geochem. Geophys. Geosyst.* **14**, 489–518.

Hart S. R. (1969) K, Rb, Cs contents and K/Rb, K/Cs ratios of fresh and altered submarine basalts. *Earth Planet. Sci. Lett.* **6**, 295–303.

Hauff F., Hoernle K. and Schmidt A. (2003) Sr-Nd-Pb composition of Mesozoic Pacific oceanic crust (Site 1149 and 801, ODP Leg 185): Implications for alteration of ocean crust and the input into the Izu-Bonin-Mariana subduction system. *Geochem. Geophys. Geosyst.* **4**, art. no.-8913.

Hegner E. and Tatsumoto M. (1987) Pb, Sr, and Nd isotopes in basalts and sulfides from the Juan-De-Fuca Ridge. *J. Geophys. Res.-Solid Earth and Planets* **92**, 11380–11386.

Hermann J. and Rubatto D. (2009) Accessory phase control on the trace element signature of sediment melts in subduction zones. *Chem. Geol.* **265**, 512–526.

Hofmann A. E., Bourg I. C. and DePaolo D. J. (2012) Ion desolvation as a mechanism for kinetic isotope fractionation in aqueous systems. *P. Natl. Acad. Sci. U.S.A.* **109**, 18689–18694.

Hofmann A. W. and White W. M. (1983) Ba, Rb and Cs in the Earth's mantle. *Z. Naturforsch.* **38**, 256–266.

Horner T. J., Kinsley C. W. and Nielsen S. G. (2015) Barium-isotopic fractionation in seawater mediated by barite cycling and oceanic circulation. *Earth Planet. Sci. Lett.* **430**, 511–522.

Horner T. J., Pryer H. V., Nielsen S. G., Crockford P. W., Gauglitz J. M., Wing B. A. and Ricketts R. D. (2017) Pelagic barite precipitation at micromolar ambient sulfate. *Nat. Commun.* **8**. Artn 1342.

Huang J., Zhang X.-C., Chen S., Tang L., Wörner G., Yu H. and Huang F. (2018) Zinc isotopic systematics of Kamchatka-Aleutian arc magmas controlled by mantle melting. *Geochim. Cosmochim. Acta* **238**, 85–101.

Ishikawa T. and Nakamura E. (1994) Origin of the slab component in arc lavas from across-arc variation of B and PB isotopes. *Nature* **370**, 205–208.

Jacquet S. H. M., Dehairs F., Savoye N., Obernosterer I., Christaki U., Monnin C. and Cardinal D. (2008) Mesopelagic organic carbon remineralization in the Kerguelen Plateau region tracked by biogenic particulate Ba. *Deep-Sea Res. Part Ii-Topical Stud. Oceanography* **55**, 868–879.

Jicha B. R. and Kay S. M. (2018) Quantifying arc migration and the role of forearc subduction erosion in the central Aleutians. *J. Volcanol. Geotherm. Res.* **360**, 84–99.

Johnson M. C. and Plank T. (1999) Dehydration and melting experiments constrain the fate of subducted sediments. *Geochem. Geophys. Geosyst.* **1**. Artn 1007.

Kay R. W. (1978) Aleutian magnesian andesites - melts from subducted Pacific ocean crust. *J. Volcanol. Geotherm. Res.* **4**, 117–132.

Kay R. W. (1980) Volcanic arc magmas - implications of a melting-mixing model for element recycling in the crust-upper mantle system. *J. Geol.* **88**, 497–522.

Kay R. W. and Kay S. M. (1988) Crustal recycling and the Aleutian arc. *Geochim. Cosmochim. Acta* **52**, 1351–1359.

Kay R. W., Sun S. S. and Lee-Hu C. N. (1978) Pb and Sr isotopes in volcanic rocks from the Aleutian Islands and Pribilof Islands, Alaska. *Geochim. Cosmochim. Acta* **42**, 263–273.

Kay S. M. and Kay R. W. (1994) Aleutian magmas in space and time. In *The Geology of Alaska* (eds. G. Plafker and H. C. Berg). Geological Society of America, pp. 687–722.

Kelley K. A., Plank T., Ludden J. and Staudigel H. (2003) Composition of altered oceanic crust at ODP Sites 801 and 1149. *Geochem. Geophys. Geosyst.* **4**.

Kessel R., Schmidt M. W., Ulmer P. and Pettke T. (2005) Trace element signature of subduction-zone fluids, melts and supercritical liquids at 120–180 km depth. *Nature* **437**, 724–727.

Klein F., Grozeva N. G., Seewald J. S., McCollom T. M., Humphris S. E., Moskowitz B., Berquo T. S. and Kahl W. A. (2015) Experimental constraints on fluid-rock reactions during incipient serpentinization of harzburgite. *Am. Mineral.* **100**, 991–1002.

Kodolanyi J., Pettke T., Spandler C., Kamber B. S. and Gmeling K. (2012) Geochemistry of ocean floor and fore-arc serpentinites: constraints on the ultramafic input to subduction zones. *J. Petrol.* **53**, 235–270.

König S., Wille M., Voegelin A. and Schoenberg R. (2016) Molybdenum isotope systematics in subduction zones. *Earth Planet. Sci. Lett.* **447**, 95–102.

Korenaga J. (2017) On the extent of mantle hydration caused by plate bending. *Earth Planet. Sci. Lett.* **457**, 1–9.

Marschall H. R. and Schumacher J. C. (2012) Arc magmas sourced from melange diapirs in subduction zones. *Nat. Geosci.* **5**, 862–867.

Miller D. M., Goldstein S. L. and Langmuir C. H. (1994) Cerium lead and lead-isotope ratios in arc magmas and the enrichment of lead in the continents. *Nature* **368**, 514–520.

Nan X.-Y., Yu H.-M., Rudnick R. L., Gaschnig R. M., Xu J., Li W.-Y., Zhang Q., Jin Z.-D., Li X.-H. and Huang F. (2018) Barium isotopic composition of the upper continental crust. *Geochim. Cosmochim. Acta* **233**, 33–49.

Nielsen S. G., Horner T. J., Pryer H. V., Blusztajn J., Shu Y., Kurz M. D. and Le Roux V. (2018) Barium isotope evidence for pervasive sediment recycling in the upper mantle. *Sci. Adv.* **4**, eaas8675.

Nielsen S. G. and Marschall H. R. (2017) Geochemical evidence for mélange melting in global arcs. *Sci. Adv.* **3**, e1602402.

Nielsen S. G., Yogodzinski G. M., Prytulak J., Plank T., Kay S. M., Kay R. W., Blusztajn J., Owens J. D., Auro M. and Kading T. (2016) Tracking along-arc sediment inputs to the Aleutian arc using thallium isotopes. *Geochim. Cosmochim. Acta* **181**, 217–237.

Paytan A. and Griffith E. M. (2007) Marine barite: Recorder of variations in ocean export productivity. *Deep-Sea Res. Part Ii-Topical Stud. Oceanography* **54**, 687–705.

Pearce J. A. and Peate D. W. (1995) Tectonic implications of the composition of volcanic arc magmas. *Annu. Rev. Earth Planet. Sci.* **23**, 251–285.

Persson I., Sandström M. and Yokoyama H. (1995) Structure of the solvated strontium and barium ions in aqueous, dimethyl

sulfoxide and pyridine solution, and crystal structure of strontium and barium hydroxide octahydrate. *Zeitschrift für Naturforschung A* **21**.

Plank T. (2005) Constraints from thorium/lanthanum on sediment recycling at subduction zones and the evolution of the continents. *J. Petrol.* **46**, 921–944.

Plank T. and Langmuir C. H. (1993) Tracing trace-elements from sediment input to volcanic output at subduction zones. *Nature* **362**, 739–743.

Plank T. and Langmuir C. H. (1998) The chemical composition of subducting sediment and its consequences for the crust and mantle. *Chem. Geol.* **145**, 325–394.

Pons M.-L., Debret B., Bouilhol P., Delacour A. and Williams H. (2016) Zinc isotope evidence for sulfate-rich fluid transfer across subduction zones. *Nat. Commun.* **7**, 13794.

Schmidt M. W. and Poli S. (1998) Experimentally based water budgets for dehydrating slabs and consequences for arc magma generation. *Earth Planet. Sci. Lett.* **163**, 361–379.

Shinjo R., Chung S.-L., Kato Y. and Kimura M. (1999) Geochemical and Sr-Nd isotopic characteristics of volcanic rocks from the Okinawa Trough and Ryukyu Arc: Implications for the evolution of a young, intracontinental back arc basin. *J. Geophys. Res.: Solid Earth* **104**, 10591–10608.

Shinjo R., Woodhead J. D. and Hergt J. M. (2000) Geochemical variation within the northern Ryukyu Arc: magma source compositions and geodynamic implications. *Contrib. Mineral. Petrol.* **140**, 263–282.

Shu Y., Nielsen S. G., Marschall H. R., John T., Blusztajn J. and Auro M. (2019) Closing the loop: subducted eclogites match thallium isotope compositions of ocean island basalts. *Geochim. Cosmochim. Acta* **250**, 130–148.

Shu Y., Nielsen S. G., Zeng Z., Shinjo R., Blusztajn J., Wang X. and Chen S. (2017) Tracing subducted sediment inputs to the Ryukyu arc-Okinawa trough system: Evidence from thallium isotopes. *Geochim. Cosmochim. Acta* **217**, 462–491.

Skora S. and Blundy J. (2010) High-pressure hydrous phase relations of radiolarian clay and implications for the involvement of subducted sediment in arc magmatism. *J. Petrol.* **51**, 2211–2243.

Solomon E. A. and Kastner M. (2012) Progressive barite dissolution in the Costa Rica forearc – Implications for global fluxes of Ba to the volcanic arc and mantle. *Geochim. Cosmochim. Acta* **83**, 110–124.

Spandler C., Mavrogenes J. and Hermann J. (2007) Experimental constraints on element mobility from subducted sediments using high-P synthetic fluid/melt inclusions. *Chem. Geol.* **239**, 228–249.

Spandler C. and Pirard C. (2013) Element recycling from subducting slabs to arc crust: A review. *Lithos* **170**, 208–223.

Staudigel H. and Hart S. R. (1983) Alteration of basaltic glass - mechanisms and significance for the oceanic-crust seawater budget. *Geochim. Cosmochim. Acta* **47**, 337–350.

Staudigel H., Plank T., White W. and Schmincke H.-U. (1996) Geochemical fluxes during seafloor alteration of the basaltic upper oceanic crust; DSDP sites 417 and 418. In *Subduction Top to Bottom* (eds. G. E. Bebout, D. W. Scholl, S. H. Kirby and J. P. Platt). AGU Monograph, pp. 19–38.

Talley L. D. (2013) Closure of the global overturning circulation through the Indian, pacific, and southern oceans schematics and transports. *Oceanography* **26**, 80–97.

Tatsumi Y. (1989) Migration of fluid phases and genesis of basalt magmas in subduction zones. *J. Geophys. Res.: Solid Earth* **94**, 4697–4707.

Tera F., Brown L., Morris J., Sacks I. S., Klein J. and Middleton R. (1986) Sediment incorporation in island-arc magmas - inferences from be-10. *Geochim. Cosmochim. Acta* **50**, 535–550.

von Allmen K., Bottcher M. E., Samankassou E. and Nagler T. F. (2010) Barium isotope fractionation in the global barium cycle: First evidence from barium minerals and precipitation experiments. *Chem. Geol.* **277**, 70–77.

von Huene R., Ranero C. s. R. and Vannucchi P. (2004) Generic model of subduction erosion. *Geology* **32**, 913–916.

Woodhead J. D., Eggins S. M. and Johnson R. W. (1998) Magma genesis in the New Britain island arc: Further insights into melting and mass transfer processes. *J. Petrol.* **39**, 1641–1668.

Workman R. K. and Hart S. R. (2005) Major and trace element composition of the depleted MORB mantle (DMM). *Earth Planet. Sci. Lett.* **231**, 53–72.

Worzewski T., Jegen M., Kopp H., Brasse H. and Castillo W. T. (2011) Magnetotelluric image of the fluid cycle in the Costa Rican subduction zone. *Nat. Geosci.* **4**, 108–111.

Wunder B., Meixner A., Romer R. L., Wirth R. and Heinrich W. (2005) The geochernical cycle of boron: Constraints from boron isotope partitioning experiments between mica and fluid. *Lithos* **84**, 206–216.

Yogodzinski G. M., Brown S. T., Kelemen P. B., Vervoort J. D., Portnyagin M., Sims K. W. W., Hoernle K., Jicha B. R. and Werner R. (2015) The role of subducted basalt in the source of island arc magmas: evidence from seafloor lavas of the western Aleutians. *J. Petrol.* **56**, 441–492.

Yogodzinski G. M., Kay R. W., Volynets O. N., Koloskov A. V. and Kay S. M. (1995) Magnesian andesite in the Western Aleutian Komandorsky region - implications for slab melting and processes in the mantle wedge. *Geol. Soc. Am. Bull.* **107**, 505–519.

Yogodzinski G. M., Kelemen P. B., Hoernle K., Brown S. T., Bindeman I., Vervoort J. D., Sims K. W. W., Portnyagin M. and Werner R. (2017) Sr and O isotopes in western Aleutian seafloor lavas: Implications for the source of fluids and trace element character of arc volcanic rocks. *Earth Planet. Sci. Lett.* **475**, 169–180.

Yogodzinski G. M., Lees J. M., Churikova T. G., Dorendorf F., Woerner G. and Volynets O. N. (2001) Geochemical evidence for the melting of subducting oceanic lithosphere at plate edges. *Nature* **409**, 500–504.

Yogodzinski G. M., Vervoort J. D., Brown S. T. and Gerseny M. (2011) Subduction controls of Hf and Nd isotopes in lavas of the Aleutian island arc. *Earth Planet. Sci. Lett.* **300**, 226–238.

Zack T., Rivers T. and Foley S. F. (2001) Cs-Rb-Ba systematics in phengite and amphibole: an assessment of fluid mobility at 2.0 GPa in eclogites from Trescolmen. *Central Alps. Contrib. Mineral. Petrol.* **140**, 651–669.

Associate editor: Fang Huang